

# Effects of activated carbon spheres with particle sizes derived from glucose by hydrothermal method on the performance of lithium-sulfur batteries

Q. WANG<sup>a</sup>, X. Y. QIAN<sup>a,\*</sup>, L. N. JIN<sup>a</sup>, X. Q. SHEN<sup>a,\*</sup>, J. L. TAN<sup>b</sup>, L WANG<sup>b</sup>

<sup>a</sup>Institute for Advanced Materials, College of Materials Science and Engineering, Jiangsu University, Zhenjiang 212013, P.R. China

<sup>b</sup>Hunan Engineering Laboratory of Power Battery Cathode Materials, Changsha Research Institute of Mining and Metallurgy, Changsha 410012, P.R. China

Carbon spheres (CSs) derived from different raw materials are proved to be good sulfur hosts for Li-S battery cathode materials. But there is little attention about activated carbon spheres (ACSSs) with different particle sizes and specific surface areas. In this paper, CSs with particle sizes were prepared with glucose by hydrothermal method and activated by KOH. Three ACSSs with particle sizes were used to load with sulfur as cathodes of Li-S batteries to analyze the effects of different specific surface areas on battery performance. Electrochemical measurements show that the larger the specific surface area and particle size, the better the battery performance.

(Received March 13, 2019; accepted February 17, 2020)

**Keywords:** Li-S battery, Activated carbon spheres, Particle sizes, Specific surface area

## 1. Introduction

With the rapid development of electronic equipment and electric vehicles, lithium-ion batteries have been unable to meet the growing demand, thus more reliable batteries owning high energy density, stable cyclic performance, and low cost are increasingly required [1]. Li-S batteries have attracted a world-wide attention because of their theoretical specific capacity (2600Wh/kg) which is several times higher than lithium-ion batteries [2,3]. Moreover, as the sulfur element is rich in natural content and friendly to the environment, Li-S batteries have a very good development prospect [4,5]. However, at present, there are still many defects in Li-S batteries which heavily constrained its development. Firstly, sulfur itself has poor electrical conductivity [6], therefore a large number of conductive additives are needed to ensure that the active materials can be fully used [7]. Secondly, the serious volume change in the process of charging and discharging [6,8], and the shuttle effect of lithium polysulfide make a rapid decay of the active sulfur [9], which are fatal for the cycle and rate performance of the Li-S batteries. Feasible approaches have been proposed to alleviate these problems, including compound cathode, modified separator, interlayer, electrolyte modification and anode protection. In terms of cathode modification, at present, the most popular strategy is use porous conductive carbon such as carbon nanotubes [10,11], carbon nanofibers [12,13], and graphene [14,15], to compound with sulfur, so as to improve the conductivity of

the active material, alleviate the shuttle effect of polysulfide and volume change of sulfur in reaction progress.

Different carbon materials have different effects on the performance of lithium-sulfur batteries due to their different structures, conductivity and specific surface area. Compared with carbon nanotubes and graphene, carbon spheres (CSs) derived from different raw materials have lower price, and the spherical appearance is benefit for the increase of tap density which is very important for the mass energy density. A few literatures reported the use of glucose hydrothermal CSs combined with sulfur as cathode of lithium sulfur battery. Niu used NS-PCSs prepared by L-cysteine and D-glucose as sulfur host, the initial discharge capacity of the battery reached 942 mAh g<sup>-1</sup> at 0.3 C [16]. Li encapsulated the sulfur in porous carbon nanospheres derived from glucose by hydrothermal method and coated with conductive polyaniline as cathode of Li-S battery, the battery delivered a discharge capacity of 881 mAh g<sup>-1</sup> at 0.2 C [17]. But there is little attention about activated carbon spheres (ACSSs) with particle sizes and specific surface areas loaded with sulfur as cathode materials. In this paper, carbon spheres with particle sizes were prepared by hydrothermal method using glucose as the raw material and activated by KOH. Through activation, there are abundant porous structures formed in the matrix of CSs and their specific surface area can be improved [18]. The as prepared porous CSs were used to load sulfur as the cathode material of Li-S batteries. The influences of CSs with particle sizes and specific surface areas on battery

performance were carefully studied by electrochemical tests including cycle performance, rate performance, EIS and CV tests.

## 2. Experimental

### 2.1. Preparation of the CSs

CSs were prepared by hydrothermal method. Glucose and water were firstly mixed evenly in a mass ratio of 1:9, then 40ml glucose aqueous solution (0.617 mol L<sup>-1</sup>) was transferred into in the autoclave (50 mL). It was found through experiments that when the temperature was 170°C and the reaction time was less than 8h, it was difficult to get carbon spheres. But when the temperature was 180°C, if the reaction time was more than 6h, the carbon spheres adhered seriously. In order to get relatively independent carbon spheres, hydrothermal reaction were carried out under three different conditions (170°C-8 h, 170°C-10 h and 180°C-6 h respectively), and the heating rate is 2°C min<sup>-1</sup>. After the hydrothermal reaction. After the hydrothermal reaction, the suspension was cooled to room temperature and centrifuged repeatedly using deionized water until the water was clear. After drying at 60°C for 12 h, the final product was obtained.

### 2.2. Activation of the CSs

The CSs were activated by KOH activation method. CSs were mixed with KOH aqueous solution (10 wt%) evenly, and the mass ratio CSs and KOH was 1:1. After a vigorous stirring, the mixture was dried in an oven at 60°C for overnight. The dried sample was then heated in the tube furnace at 800°C for 2 h in N<sub>2</sub> atmosphere with the heating rate of 2°C/min followed by a natural cooling process. After the heat treatment, the activated sample was washed with HCl aqueous solution (10 wt%) to remove residual KOH and then centrifuged and washed to neutral using deionized water. The end product was obtained by drying the precipitate in oven for 12 h.

### 2.3. The preparation of cathode and cell assembly

The as prepared ACSs and sulfur was mixed in the mass ratio of 1:4 and grind in the agate jar using the hydro-ball-milling technique. The mixture was then sealed

in a reactor and heated at 155°C for 12 h to obtain C/S composite. The slurry of the cathode electrode for Li-S battery was prepared by mixing C/S composite, KB (Ketjen Black, a kind of conductive carbon) and La133 in the weight ratio of 7:2:1 using water as the dispersant. The cathode slurry was coated on an aluminum foil by an automatic coating machine and dried in vacuum oven for 12 h at 60°C. The average mass density of the sulfur in the cathode was estimated to be 1-1.5 mg cm<sup>-2</sup>. Half-cells were assembled in a glove box (Mikrouna) filled with Ar atmosphere, polyethylene diaphragm was used as the separator, 1,3-dioxolane (DOL) and dimethoxymethane (DME) mixed by the volume ratio of 1:1 with 1 M LiTFSI and 2% LiNO<sub>3</sub> addition was used as the electrolyte.

## 3. Results and discussion

### 3.1. Characterization of materials

The particle size of CSs was measured by laser particle size analyzer (MS 3000). The microstructural characterizations were carried out via X-ray diffraction (XRD, D/max 2550 diffractometer). The XRD analysis was operated from 10° to 90° with a step of 10° min<sup>-1</sup>.The porous structures and surface morphology of CSs and the ACSs was carried out by field emission scanning electron microscopy (FE-SEM, JSM-7800F), and ACSs was tested by transmission electron microscopy (TEM, JEOL JEM 2100F). Specific surface area and pore size analyzer (BET Quantachrome autosorb Iq3) were used to analyze the specific surface areas and pore size distribution of the ACSs and ACSs/S-A.

The particle sizes of CSs are shown in Fig. 1. Carbon microspheres with different particle sizes were obtained by changing the hydrothermal temperature and time. Under the conditions of 170°C-10h, 180°C-6h, 170°C-8h, the average particle size of CSs are 674 nm, 364 nm and 130 nm. We can find that when raising reaction time or temperature, the particle size of carbon spheres will increase and the distribution range will become wider. The average particle size of CSs was used to distinguish the different samples in the following paragraphs. ACSs were labeled as A,B,C according to the average particle size of CSs from large to small and ACSs/S-A,B,C were used to mark different C/S composites.

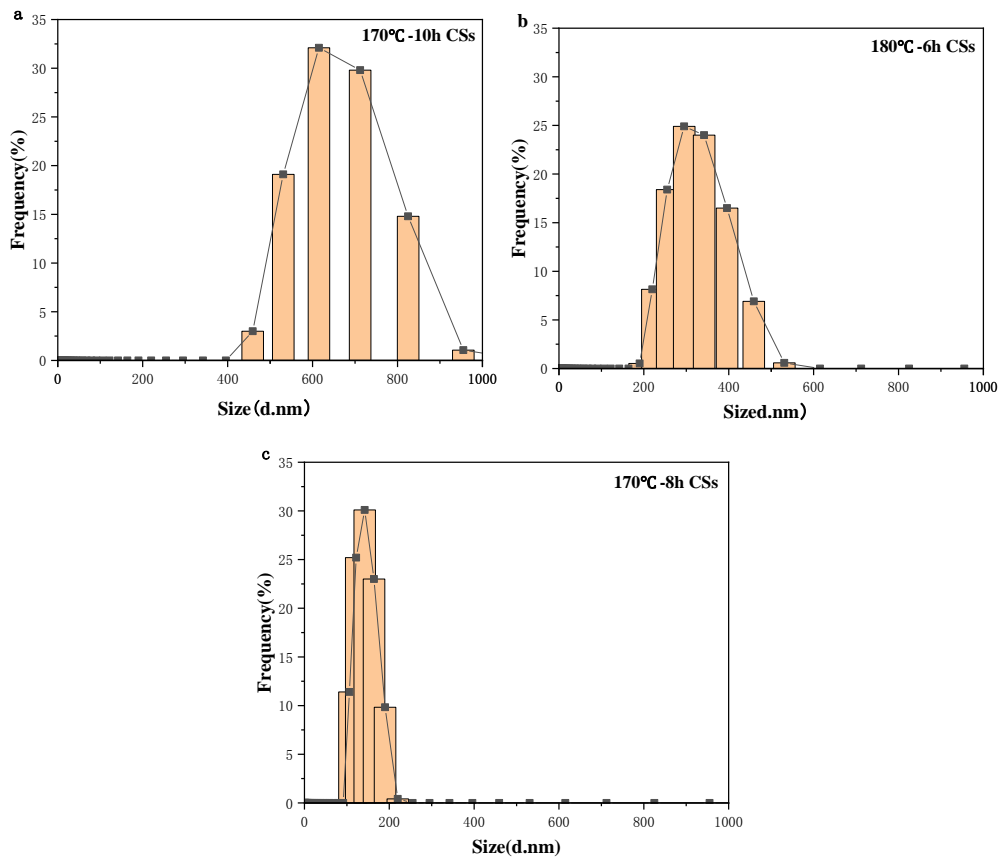


Fig. 1. Particle sizes of CSs under different conditions.  
a. 170°C-10h, b. 180°C-6h, c. 170°C-8h (color online)

The XRD patterns are shown in Fig. 2. The XRD analysis of ACSs-A and ACSs/S-A composites was operated at 20 mA and 40 KV using Cu K $\alpha$  radiation from 10° to 90° with a step of 10° min<sup>-1</sup>. The XRD pattern of ACSs-A has two broad peaks of (002) plane and (100) plane which belong to graphitized carbon [3].

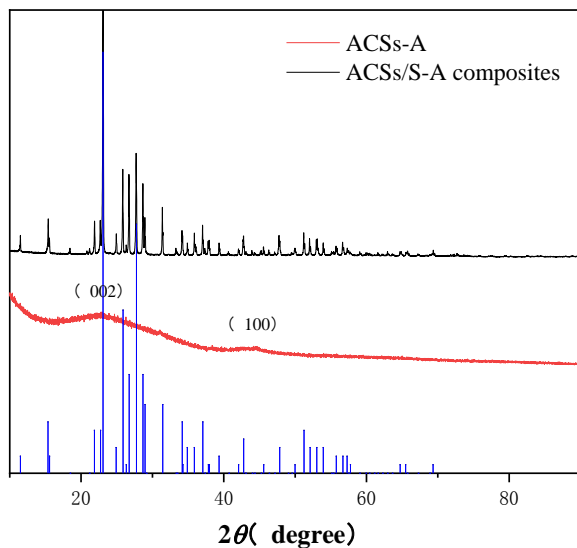


Fig. 2. XRD patterns of ACSs-A and ACSs/S-A (color online)

At the bottom of the figure is the diffraction standard card (JCPDS PDF 08-0247) of sulfur. In the XRD diffraction pattern of ACSs/S-A composites, the diffraction peak of carbon and sulfur was found and the diffraction peak of sulfur in ACSs/S-A composites is consistent with the diffraction pattern of elemental sulfur. It shows that sulfur also exists in rhombic structure in the complex, which means the crystal structure of sulfur was not destroyed by ball-milling and hot melt. The sulfur and porous carbon spheres were well mixed.

The Raman spectrum of pure sulfur, ACSs-A and ACSs/S-A composites are shown in Fig. 3. Four peaks of pure sulfur at around 471, 215, 151, 82 cm<sup>-1</sup>, indicate the S-S bond of molecular S8. The D-bands (disorder-induced phonon mode) of ACSs-A and ACSs/S-A severally are at about 1364 and 1348 cm<sup>-1</sup>, while the G-bands (graphite band) of ACSs-A and ACSs/S-A are all at about 1581 cm<sup>-1</sup>. The value of the D and G band (ID/IG) for ACSs-A is about 0.978, indicating a relative high degree of graphitic structure [19]. Additionally, the Raman spectra of ACSs/S-A show several peaks between 0-500 cm<sup>-1</sup>, demonstrating the existing of sulfur, which is consistent with the XRD results.

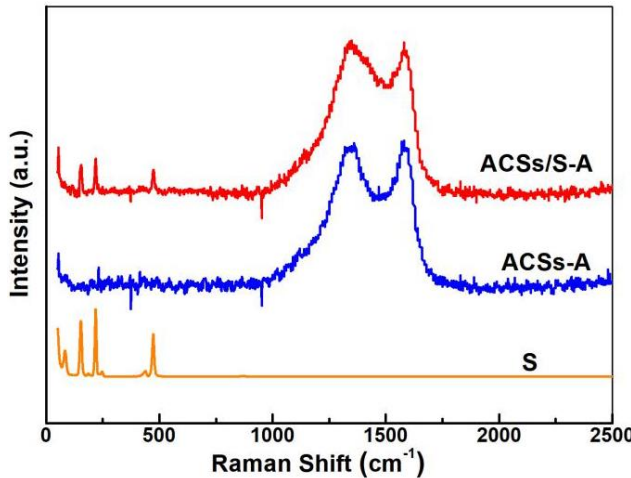


Fig. 3. Raman spectra of S, ACSS-A and ACSS/S-A (color online)

Scanning electron microscopy (SEM) images are shown in Fig. 4. Fig. 4. a, b and c are CSs prepared by hydrothermal method. SEM images show that the degree of spheroidization of carbon microspheres is relatively high and the surface of the CSs is smooth. The sizes of the carbon spheres are almost consistent with the results of particle size analysis. Raising the hydrothermal time or temperature will increase the size of the CSs. ACSS after KOH activation are shown in picture d, e, f. The ACSSs with large particle size can still remain a spherical appearance and have plenty of pores in the sphere matrix, while the ACSSs with small particle size are more easily broken, which is caused by the intense activation reaction of KOH [17]. When too many CSs were etched by KOH, it would easily lead to the collapse of the structure. Image g is SEM of ACSS/S-A, we can still see the profile of ACSSs. The porous carbon spheres are solid, so the sulfur is mainly distributed in the surface and pores after loading with sulfur.

Fig. 5 shows the TEM and HRTEM image of ACSS-A, it possess abundant pores in the sphere matrix which means a large specific surface area. Therefore it will more benefit for the infiltration of electrolyte and provide more active sites and storage space for sulfur to improving the utilization rate of active materials and battery performance [20]. Abundant pore structure and high specific surface area can also bind sulfur well and have physical adsorption effect on polysulfide, which can effectively inhibit the shuttle of polysulfide and improve the cycling stability of the battery [3,21].

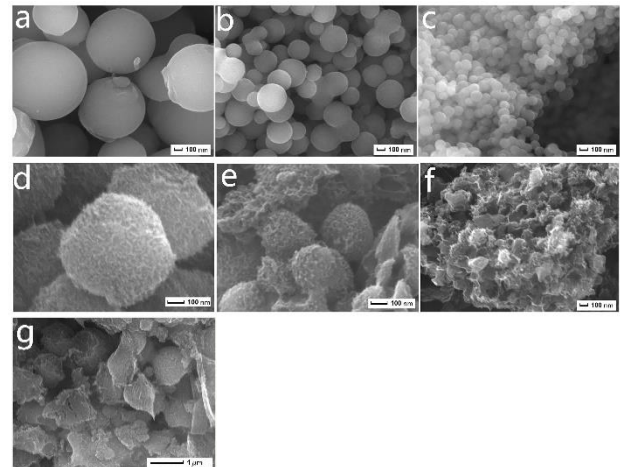


Fig. 4. SEM of CSs. a. CSs-A. b. CSs-B. c. CSs-C. SEM of ACSS .d. ACSS-A. e. ACSS-B. f. ACSS-C. g. ACSS/S-A

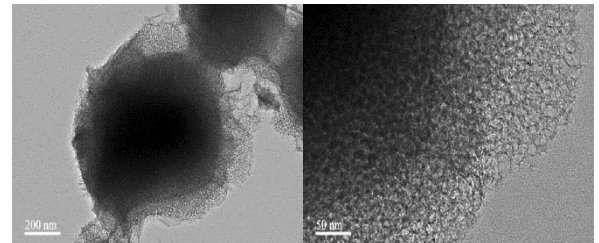


Fig. 5. TEM of ACSS-A

In order to verify that sulfur and ACSSs were well compounded, EDS mapping was made for ACSS/S-A, which is showed in Fig. 6. We can find carbon and sulfur elements in composites, and the distribution is relatively uniform, which proves that carbon and sulfur was combined well.

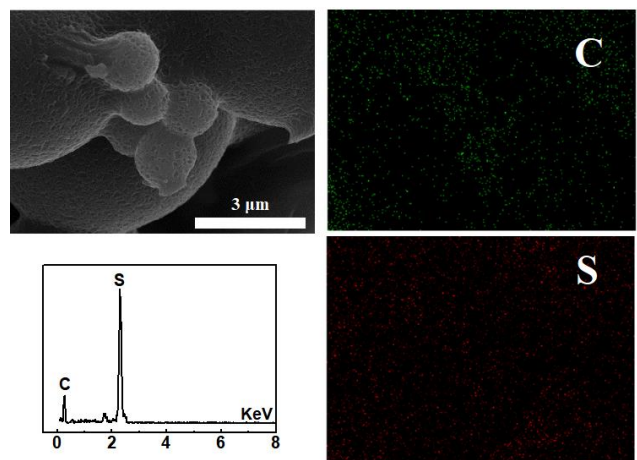


Fig. 6. EDS mapping of ACSS/S-A (color online)

And in order to determine the content of sulfur in the composites, TG analysis was performed in Fig. 7 because of the great influence of sulfur content on the performance of Li-S batteries. In the atmosphere of N<sub>2</sub>, we heated the ACSs/S-A to 600°C at 10°C/min. As shown in Fig. 7, TG curves demonstrate that the sulfur weight loss ratio is 82.01%, 81.37% and 82.24% respectively, which is basically consistent with the experimental design. The extra part of sulfur could be caused by the reunion in the mixing process.

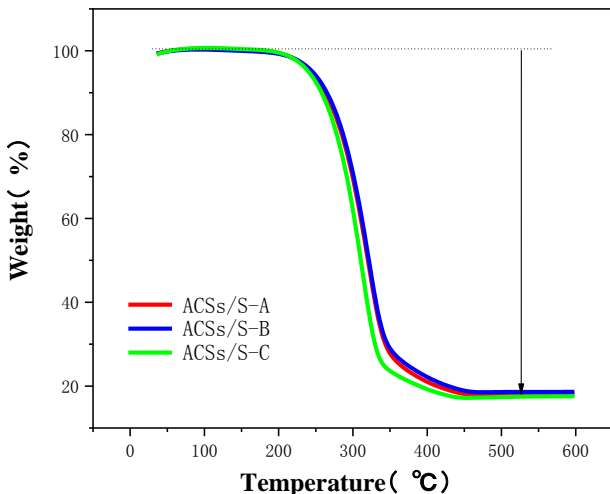


Fig. 7. TG of ACSs/S-A, B and C (color online)

Fig. 8.a shows N<sub>2</sub> adsorption-desorption isotherms of the three ACSs sample. The specific surface area was calculated using the Brunauer-Emmett-Teller (BET) method. The BET surface areas of ACSs-A, B, C are 1633.95 m<sup>2</sup> g<sup>-1</sup>, 431.98 m<sup>2</sup> g<sup>-1</sup> and 431.5 m<sup>2</sup> g<sup>-1</sup> respectively. Pore volumes are 2.291 cm<sup>3</sup> g<sup>-1</sup>, 0.655 cm<sup>3</sup> g<sup>-1</sup> and 0.608 cm<sup>3</sup> g<sup>-1</sup> correspondingly. It has been proved that high specific surface area and large pore volume can contribute to high sulfur loading, effective electrolyte infiltration and fine accommodating of the volume change [22]. Apparently, the ACSs-A has a largest specific surface area and pore volume which is supposed to have the best electrochemical performances. The BJH pore size distribution curves of the ACSs in Fig. 8.b indicates that the pore size of most holes is less than 2 nm, which means micropore, ACSs-A and B has a small amount of small mesopores [23] from 3 to 6nm.

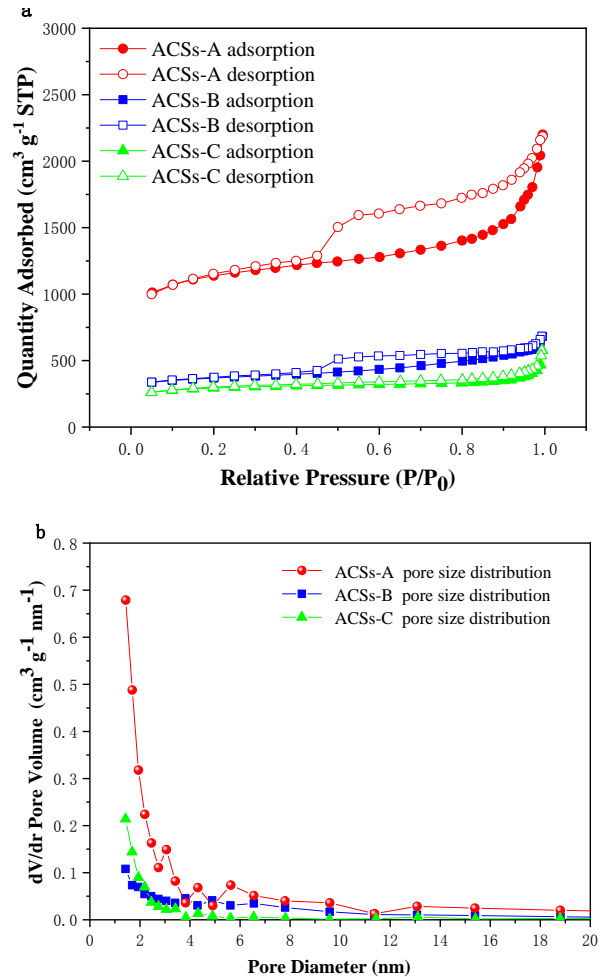


Fig. 8. a. N<sub>2</sub> adsorption-desorption isotherms. b. BJH pore size distribution of the ACSs (color online)

### 3.2. Electrochemical properties

The galvanostatic charge/discharge, CV, and EIS tests were carried out to compare the electrochemical properties of different Li-S batteries using different ACSs/S cathode.

As shown in Fig. 9 a, the cycle performance of Li-S batteries with different cathode is tested at the current density of 0.5 C (1 C = 1675 mA g<sup>-1</sup>) from 1.7 to 2.8 V. The initial discharge capacities of the three batteries at 0.5 C are 713.6 mAh g<sup>-1</sup> (ACSs/S-A cathode), 615.2 mAh g<sup>-1</sup> (ACSs/S-B cathode) and 537.4 mAh g<sup>-1</sup> (ACSs/S-C cathode) respectively. After 300 cycles, the discharge capacities of the three batteries are 490.5 mAh.g<sup>-1</sup>(ACSs/S-A cathode), 330.1 mAh g<sup>-1</sup>(ACSs/S-B cathode) and 312.2 mAh g<sup>-1</sup>(ACSs/S-C cathode) respectively. The capacity retention rates are 68.7%, 61.4% and 50.7% correspondingly, and the columbic efficiencies are all more than 97%. obviously that the battery using ACSs/S-A cathode has the best charging and discharging cycle performance, which is mainly attributed to the largest specific surface area and pore volume of ACSs-A. The mesopores of ACSs-A can load more active sulfur and the micropores are beneficial to the adsorption

of lithium polysulfide, thus the capacity and the cycle retention are improved simultaneously.

Fig. 9 b shows the rate performance of the three batteries. Obviously the ACSs/S-A cathode sample has better rate capability, with the discharge capacity of  $611.1 \text{ mAh g}^{-1}$ ,  $561.6 \text{ mAh g}^{-1}$  and  $459.7 \text{ mAh g}^{-1}$  at 0.5 C, 1 C and 2 C, respectively. When the discharge rate returns to 0.5 C, the specific capacity retention of the ACSs/S-A cathode are approximately 100%. In comparison, the ACSs/S-B cathode sample and ACSs/S-C cathode sample only possess the specific capacity retention of 95% and 87.5%. The results proved that the ACSs/S-A cathode sample has the best rate capability.

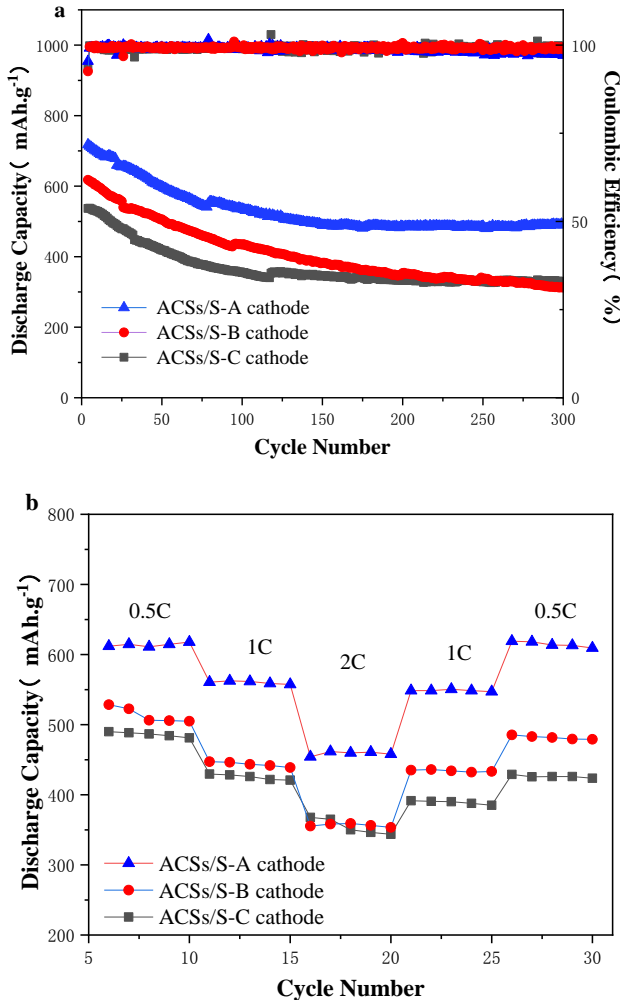


Fig. 9. Cycle(a) and rate(b) performance of batteries with ACSs/S-A cathode, ACSs/S-B cathode, ACSs/S-C cathode (color online)

Cyclic voltammograms (CV) of different Li-S cells with ACSs/S-A, ACSs/S-B and ACSs/S-C cathode were obtained over a voltage range from 1.7 to 2.8 V under a scan rate of 0.1 mV s<sup>-1</sup>, and the CV curves are shown in Fig. 10. There are two peaks at around 2.3 and 2.0V respectively in the CV curves, which are two reduction peaks representing two reduction reactions of the conversion of S<sub>8</sub> to soluble lithium polysulfides (Li<sub>2</sub>S<sub>x</sub>, 4

$\leq x \leq 8$ ) and further conversion of soluble lithium polysulfides to insoluble Li<sub>2</sub>S<sub>2</sub>/Li<sub>2</sub>S [8,24]. On the contrary, the peaks at around 2.4 V, which are oxidation peaks representing the reversible process of the above reactions. Moreover, we can find that the reduction potential of the ACSs/S-A cathode is 2.02V, which is a little bit higher than that of the others (2.01V, 2.0V) on the CV curves. The high reduction potential indicates that the ACSs/S-A cathode material is more favorable for the electrochemical kinetics [25].

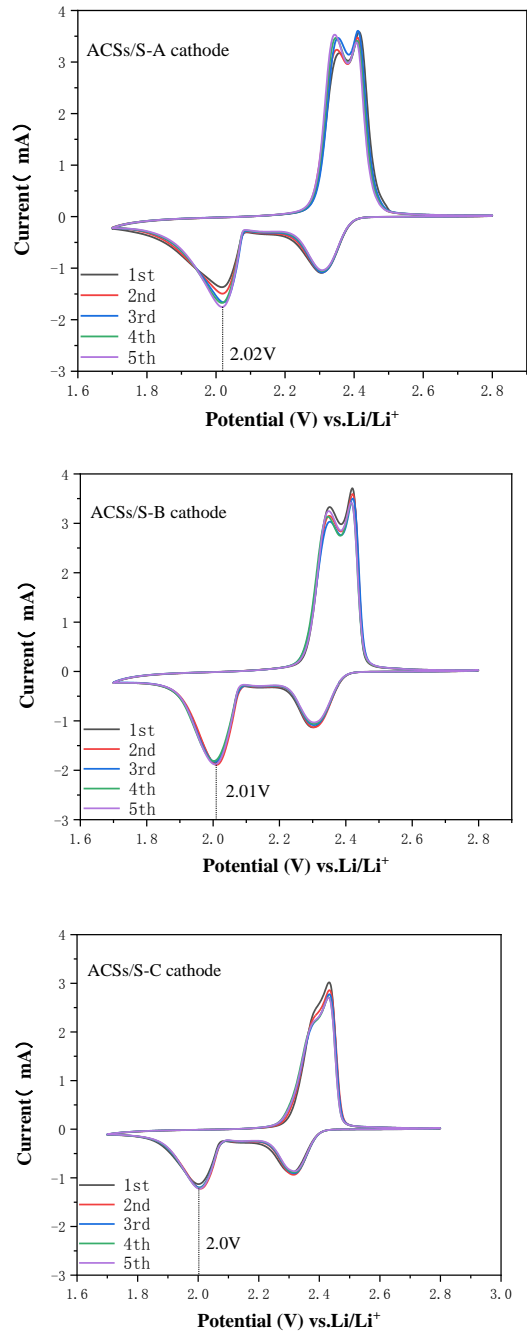


Fig. 10. CV of cells with ACSs/S-A cathode, ACSs/S-B cathode, ACSs/S-C cathode (color online)

EIS was used to make further comparisons of Li-S batteries assembled of different cathodes with frequency

from 0.01 Hz to 100 KHz at open circuit potential before the cycling performance test and to deeply investigate the internal electrochemical behaviors. As shown in Fig. 11, the Nyquist plots include an intercept, a depressed semicircle, and an inclined line. The intercept at high frequency region on the real axis  $Z'$  corresponded to the resistance of electrolyte ( $R_s$ ) [26]. The depressed semicircle from high to intermediate frequency region represented the charge transfer resistance ( $R_{ct}$ ) [27] on the sulfur electrode. Table 1 lists the impedance parameters of different cells. The  $R_{ct}$  of different cells are 26.51  $\Omega$  (ACSS/S-A), 28.80  $\Omega$  (ACSS/S-B) and 32.50  $\Omega$  (ACSS/S-C). The  $R_{ct}$  of ACSS/S-A cathode cell is the smallest, which proves that the cell with ACSS/S-A cathode is more beneficial to Li<sup>+</sup> transport. And it agreed well with the results of cycling performance, rate capability, and CV measurements.

Table 1. Impedance parameters of different cells

samples	$R_s$ ( $\Omega$ )	$R_{ct}$ ( $\Omega$ )
ACSS/S-A	2.52	26.51
ACSS/S-B	2.44	28.80
ACSS/S-C	2.03	32.50

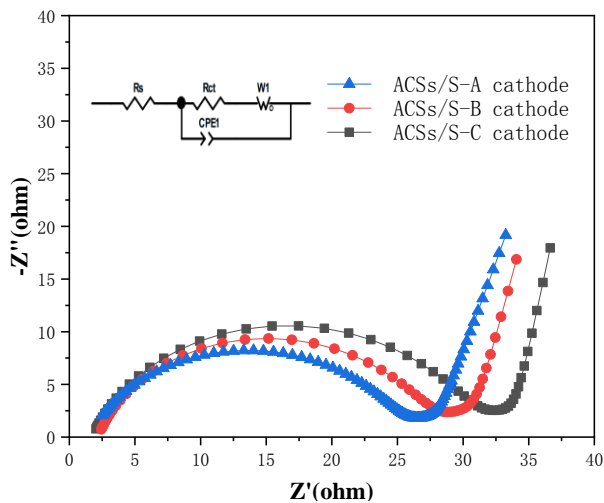


Fig. 11. EIS of cells with ACSS/S-A cathode, ACSS/S-B cathode, ACSS/S-C cathode (color online)

#### 4. Conclusion

In summary, specific surface area and pore volume are important factors to be considered when choosing or preparing cathode materials for Li-S batteries. In this paper, glucose was used as raw material to prepare CSs by hydrothermal method. By changing the hydrothermal temperature and time, CSs with three different diameters were obtained, the average particle size of CSs-A, B, C are 674 nm, 364 nm and 130 nm respectively. Then after

activation, the matrix of the CSs was improved with many holes and the specific surface area increased. The specific surface areas of ACSSs-A, B, C are 1633.95  $m^2 g^{-1}$ , 431.98  $m^2 g^{-1}$  and 431.5  $m^2 g^{-1}$  respectively and the pore volumes are 2.291  $cm^{-3} g^{-1}$ , 0.655  $cm^{-3} g^{-1}$  and 0.608  $cm^{-3} g^{-1}$  respectively. Abundant pore structures can be seen from SEM and TEM images. However, as a result of potassium hydroxide violent activation reaction. The spherical structure of small particle size CSs were seriously damaged. The three ACSSs loaded with sulfur were used as cathodes for batteries tests. After comprehensive comparison, it is found that the larger specific surface area of the sample is, the better its electrochemical performance will be. This is mainly because the larger specific surface area and pore volume are more conducive to the infiltration of the electrolyte, which can provide more active sites and reduce the polarization, thus improving the utilization rate of the active material and the performance of the batteries.

#### Acknowledgements

We acknowledge the financially supported by the Youth Fund of Jiangsu Province (Grant No. BK20190857) and the Start-up Fund of Jiangsu University (Grant No.14JDG060, 14JDG058).

#### References

- [1] H. Zhang, Q. Gao, W. Qian, H. Xiao, Z. Li, L. Ma, X. Tian, ACS Appl. Mater. Inter. **10**, 18726 (2018).
- [2] A. B. Puthirath, A. Baburaj, K. Kato, D. Salpekar, N. Chakingal, Y. Cao, P. M. Ajayan, Electrochimica Acta **306**, 489 (2019).
- [3] S. Wang, X. Qian, L. Jin, D. Rao, S. Yao, X. Shen, S. Qin, J. Solid. State. Electr. **21**, 3229 (2017).
- [4] X. Liang, Z. Wen, Y. Liu, H. Zhang, L. Huang, J. Jin, J. Power. Sources **196**, 3655 (2011).
- [5] Y. Q. Lu, Y. J. Wu, T. Sheng, X. X. Peng, Z. G. Gao, S. J. Zhang, Y. Zhou, ACS Appl. Mater. Inter. **10**, 13499 (2018).
- [6] C. Zhang, H. B. Wu, C. Yuan, Z. Guo, X. W. Lou, Angew. Chem. **124**, 9730 (2012).
- [7] S. Urbonaite, P. Novák, J. Power. Sources **249**, 497 (2014).
- [8] Y. Zhang, X. Zong, L. Zhan, X. Yu, J. Gao, C. Xun, P. Li, Y. Wang, Electrochim. Acta **284**, 89 (2018).
- [9] N. Jayaprakash, J. Shen, S. S. Moganty, A. Corona, L. A. Archer, Angew. Chem. Int. Edit **50**, 5904 (2011).
- [10] G. Zhou, D. W. Wang, F. Li, P. X. Hou, L. Yin, C. Liu, H. M. Cheng, Energ. Environ. Sci. **5**, 8901 (2012).
- [11] L. Ma, H. L. Zhuang, S. Wei, K. E. Hendrickson, M. S. Kim, G. Cohn, L. A. Archer, ACS Nano **10**, 1050 (2015).
- [12] Z. Li, J. Zhang, X. W. Lou, Angew. Chem. Int. Edit.

54, 12886 (2015).

- [13] S. Xue, S. Yao, M. Jing, L. Zhu, X. Shen, T. Li, Y. Liu, *Electrochim Acta*, **299**, 549 (2019).
- [14] X. Jia, C. Zhang, J. Liu, W. Lv, D. W. Wang, Y. Tao, Z. Li, Q. H. Yang, *Nanoscale* **8**, 4447 (2016).
- [15] G. Zhou, Design, Fabrication and Electrochemical Performance of Nanostructured Carbon Based Materials for High-Energy Lithium–Sulfur Batteries, Springer, Singapore, pp. 75 (2017).
- [16] S. Niu, W. Lv, G. Zhou, Y. He, B. Li, Q. H. Yang, F. Kang, *Chem. Commun.* **51**, 17720 (2015).
- [17] X. Li, M. Rao, W. Li, J. Solid. State Electr. **20**, 153 (2016).
- [18] M. Li, W. Li, S. Liu, *Carbohydr. Res.* **346**, 999 (2011).
- [19] J. Song, C. Zhang, X. Guo, J. Zhang, L. Luo, H. Liu, G. Wang, *J. Mater. Chem. A* **6**, 16610 (2018).
- [20] W. Yuan, Y. Zhang, L. Cheng, H. Wu, L. Zheng, D. Zhao, *J. Mater. Chem. A* **4**, 8932 (2016).
- [21] Y. Yan, M. Shi, Y. Wei, C. Zhao, M. Carnie, R. Yang, Y. Xu, *J. Alloys. Compd.* **738**, 16 (2018).
- [22] Q. Wang, X. Liang, W. Qiao, C. Liu, X. Liu, L. Zhan, L. Ling, *Fuel. Process. Technol.* **90**, 381 (2009).
- [23] J. B. Yang, L. C. Ling, L. Liu, F. Y. Kang, Z. H. Huang, H. Wu, *Carbon* **40**, 911 (2002).
- [24] R. Fang, S. Zhao, P. Hou, M. Cheng, S. Wang, H. M. Cheng, F. Li, *Adv. Mater.* **28**, 3374 (2016).
- [25] X. Qian, L. Jin, D. Zhao, X. Yang, S. Wang, X. Shen, X. Xi, *Electrochim. Acta* **192**, 346 (2016).
- [26] Y. Yan, Y. Wei, Q. Li, M. Shi, C. Zhao, L. Chen, Y. Xu, *J. Mater. Sci- Mater. El.* **29**, 11325 (2018).
- [27] W. Wahyudi, Z. Cao, P. Kumar, M. Li, Y. Wu, M. N. Hedhili, J. Ming, *Adv. Funct. Mater.* **28**, 1802244 (2018).

\*Corresponding authors: qianxy@ujs.edu.cn  
shenxq@ujs.edu.cn